Dynamic Walking with Footstep Adaptation on the MIT Humanoid via Linear Model Predictive Control

Yanran Ding[1], Charles Khazoom[1], Matthew Chignoli[1] and Sangbae Kim[1]

Abstract— This paper proposes a model predictive control (MPC) framework for realizing dynamic walking gaits on the MIT Humanoid. In addition to adapting footstep location and timing online, the proposed method can reason about varying height, contact wrench, torso rotation, kinematic limit and negotiating uneven terrains. Specifically, a linear MPC (LMPC) optimizes for the desired footstep location by linearizing the single rigid body dynamics with respect to the current footstep location. A low-level task-space controller tracks the predicted state and control trajectories from the LMPC to leverage the full-body dynamics. Finally, an adaptive gait frequency scheme is employed to modify the step frequency and enhance the robustness of the walking controller. Both LMPC and task-space control can be efficiently solved as quadratic programs (QP), and thus amenable for real-time applications. Simulation studies where the MIT Humanoid traverses a wave field and recovers from impulsive disturbances validated the proposed approach.

Paper Type – Recent Work [1], under review
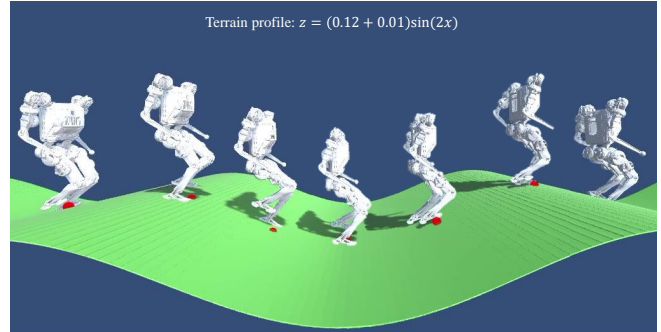*Video* – https://www.youtube.com/watch?v=uZKZeOnrJ2g

Fig. 1: Snapshots of the MIT Humanoid traversing a wave field. The red dots on the terrain indicate the desired footstep locations produced by the linear MPC.

I. INTRODUCTION

Stepping strategy is one of the most critical considerations for stable bipedal walking control, especially in the presence of external disturbances and on uneven terrains. Humanoid robots should rapidly plan footsteps that help regulate center of mass position and torso orientation to avoid falling. Those footsteps should respect kinematic limits and account for terrain irregularities. However, simultaneously fulfilling these potentially conflicting requirements in real-time is still not trivial.

The Linear Inverted Pendulum Model (LIPM) [2] is widely used for bipedal walking control, where the robot is treated as a point mass moving with constant height. Leveraging the analytical solutions of LIPM, center of mass (CoM) trajectories can be generated from Zero Moment Point [3] based control methods [4] [5]. Despite the success of this method, applying it on non-flat terrain requires substantial modification [6]. The capture point (CP) is a point on the ground where a biped can step on to come to a stop. Under the assumption of LIPM, the CP has a closed-form analytical solution [7]. The inertial effect of torso and limbs is approximated by the LIPM with flywheel model [8], [9]. However, regulating the flywheel with a bang-bang controller may not be a practical method due to limited actuator bandwidth. The CP-based method has also been extended to the cases of varying terrain heights [10] and non-linear CoM path [11] without accounting for angular momentum.

[1]The authors are with the Department of Mechanical Engineering at the Massachusetts Institute of Technology, MA - 02139, USA. email: {yanran, ckhaz, chignoli, sangbae}@mit.edu

Model Predictive Control (MPC) with footstep adaptation has been recently explored in nonlinear MPC (NMPC) [12] and Regularized Predictive Control (RPC) [13]. The major advantage is the capability to consider stepping, rotational dynamics and kinematic limits in a unified optimization framework. Nevertheless, both NMPC and RPC involve solving a nonlinear program (NLP), which is challenging to solve with on-board computation at a high rate. Real-time non-linear MPC requires extensive tuning, and the optimization can get stuck at undesirable local minima. As an alternative to solving an NLP, mixed-integer convex program (MICP) is applied on quadruped locomotion in [14] to approximate the bilinear term from the cross product of contact location and GRF with McCormick envelope [15]. Although MICP grants a global optimality certificate, the solve time grows exponentially with the number of binary variables, making it unsuitable for real-time applications.

The main contribution of this paper is a humanoid walking controller that optimizes the next step location with a linear model predictive controller (LMPC), which can be reliably solved in real-time as a QP [16]. The LMPC can reason about footstep, varying CoM height, rotational dynamics, kinematic limit and uneven terrain within a unified framework. The state and control inputs from LMPC are processed by a finite state machine and posed as tracking tasks passed to a Task-Space Controller (TSC) [17] to leverage the full-body dynamics of the humanoid. The joint torque from the TSC is applied in the humanoid dynamics simulator. In addition, a heuristic gait frequency adaptation scheme is employed to enhance the robustness of the walking controller.

II. LINEAR MPC WITH STEP LOCATION ADAPTATION

This section details how the canonical LMPC is adapted to reason about multiple aspects of bipedal walking, in particular footstep location, in a unified optimization framework. The LMPC can be formulated as an optimization problem with quadratic objective and linear constraints

$$
\begin{aligned}
\min_{\boldsymbol{u}_k, \boldsymbol{x}_k} \quad & \ell_N(\boldsymbol{x}_N) + \sum_{k=0}^{N-1} \ell_k(\boldsymbol{x}_k, \boldsymbol{u}_k) \\
\text{s.t.} \quad & \boldsymbol{x}_{k+1} = \boldsymbol{A}\boldsymbol{x}_k + \boldsymbol{B}\boldsymbol{u}_k \\
& \boldsymbol{x}_k \in \mathbb{X}, \boldsymbol{u}_k \in \mathbb{U}, k = 0, \cdots, N-1 \\
& \boldsymbol{x}_0 = \boldsymbol{x}(t),
\end{aligned} \tag{1}
$$

where $\boldsymbol{x} \in \mathbb{R}^n$ and $\boldsymbol{u} \in \mathbb{R}^m$ denote the state and control variables, respectively; N is the prediction horizon and k indicates the time step; ℓ_N and ℓ_k are the quadratic terminal and stage costs, respectively; $\boldsymbol{A}$ and $\boldsymbol{B}$ are constant matrices that propagate the discrete linear dynamics through the prediction horizon as a linear time-invariant (LTI) system; polyhedron sets $\mathbb{X}$ and $\mathbb{U}$ delineate the linear inequality constraints on the state and control, respectively.

A. System Modeling

The robot system dynamics is considered as a single domain hybrid system. The continuous dynamics concern the SRB template, and the discrete jump captures the effect of taking a step. The hybrid system Σ is defined as

$$
\Sigma : \begin{cases} \dot{\boldsymbol{x}} = \boldsymbol{f}(\boldsymbol{x}, \boldsymbol{u}), t \notin \mathcal{S}, \\ \boldsymbol{x}^+ = \Delta(\boldsymbol{x}^-), t \in \mathcal{S}, \end{cases} \tag{2}
$$

where the continuous-time dynamics is $\dot{\boldsymbol{x}} = \boldsymbol{f}(\boldsymbol{x}, \boldsymbol{u})$; the discrete transition $\boldsymbol{x}^+ = \Delta(\boldsymbol{x}^-)$ maps the state $\boldsymbol{x}^-$ to $\boldsymbol{x}^+$ on the guard of the hybrid system $\mathcal{S}$. In this work, $\mathcal{S}$ is the stepping time within the prediction horizon, which is determined by a gait schedule. For simplicity, the robot is assumed to be always in single support phase with zero aerial phase. The step location change is assumed to be instantaneous and has no immediate effect on the CoM positon and velocity.

During the continuous-time domain of (2), the SRB model is utilized to model the MIT Humanoid. Despite the design effort to place the heavy actuators close to the torso [18], the inertial effect of moving limbs is not negligible. Nevertheless, the composite inertia varies by less than 15% during walking; the dominating effect is the SRB dynamics

$$
\dot{\boldsymbol{x}} = \frac{\mathrm{d}}{\mathrm{d}t} \begin{bmatrix} \boldsymbol{p}_c \\ \boldsymbol{\Theta} \\ \dot{\boldsymbol{p}}_c \\ \dot{\boldsymbol{\Theta}} \\ \boldsymbol{c} \end{bmatrix} = \begin{bmatrix} \dot{\boldsymbol{p}}_c \\ \dot{\boldsymbol{\Theta}} \\ M^{-1}(\boldsymbol{F} + \boldsymbol{a}_g) \\ {}^{B}\boldsymbol{I}^{-1}((\boldsymbol{c} - \boldsymbol{p}_c) \times \boldsymbol{F} + \boldsymbol{m}) \\ \boldsymbol{0} \end{bmatrix}, \tag{3}
$$

where $\boldsymbol{p}_c \in \mathbb{R}^3$ is the CoM location; $\boldsymbol{\Theta} \in \mathbb{R}^3$ is the roll-pitch-yaw angle representation of the robot torso; $\boldsymbol{c} \in \mathbb{R}^3$ is the current step location, where the contact foot produces a wrench $\boldsymbol{u} = [\boldsymbol{F}^\top, \boldsymbol{m}^\top]^\top$; $\boldsymbol{a}_g = [0, 0, -g]^\top$ is the gravitational acceleration vector; M is the lumped mass and

${}^{B}\boldsymbol{I}$ is the constant inertial tensor expressed in the body frame. Note that the state $\boldsymbol{x}$ is augmented with the current step location $\boldsymbol{c}$, which is at the origin of the foot frame. The ground reaction wrench (GRW) $\boldsymbol{u}$ is comprised of force $\boldsymbol{F} \in \mathbb{R}^3$ and moment $\boldsymbol{m} \in \mathbb{R}^3$, which are applied at $\boldsymbol{c}$.

B. Discrete Linear Dynamics

The nonlinear dynamics $\boldsymbol{f}$ defined in (3) is linearized and discretized through forward Euler integration as

$$
\boldsymbol{x}_{k+1} = \boldsymbol{A}\boldsymbol{x}_k + \boldsymbol{B}\boldsymbol{u}_k + \boldsymbol{d}. \tag{4}
$$

The matrices $\boldsymbol{A}, \boldsymbol{B}, \boldsymbol{d}$ are defined as follows

$$
\boldsymbol{A} = \boldsymbol{1} + T_s \cdot \frac{\partial \boldsymbol{f}}{\partial \boldsymbol{x}}\bigg|_t \in \mathbb{R}^{n \times n} \tag{5}
$$

$$
\boldsymbol{B} = T_s \cdot \frac{\partial \boldsymbol{f}}{\partial \boldsymbol{u}}\bigg|_t \in \mathbb{R}^{n \times m} \tag{6}
$$

$$
\boldsymbol{d} = T_s \cdot \boldsymbol{f}(\boldsymbol{x}_t, \boldsymbol{u}_t) - \boldsymbol{A}\boldsymbol{x}_t - \boldsymbol{B}\boldsymbol{u}_t \in \mathbb{R}^n, \tag{7}
$$

where T_s is the prediction time step; $\boldsymbol{1}$ is the identity matrix; $\boldsymbol{x}_t, \boldsymbol{u}_t$ are the state and control vector at the current time.

C. Step Location Adaptation

Augmenting the state with $\boldsymbol{c}$ allows the MPC to reason about stepping strategy in a unified optimization framework. Specifically, the effect of taking a step $\delta\boldsymbol{c}$ on the dynamics can be quantified as $\boldsymbol{A}_c\delta\boldsymbol{c}$, where $\boldsymbol{A}_c \in \mathbb{R}^{n \times 3}$ is the last three columns of $\boldsymbol{A}$.

Unlike the control $\boldsymbol{u}_k$, which is present at every k, $\delta\boldsymbol{c}$ only appears when there is a scheduled stepping. Based on the gait schedule and current gait phase, a boolean vector $\boldsymbol{\eta} \in \{0, 1\}^N$ is introduced, where $\eta_k = 1$ indicates a scheduled step and $\eta_k = 0$ otherwise. The discrete linear dynamics (4) is updated to take into account of stepping

$$
\boldsymbol{x}_{k+1} = \boldsymbol{A}\boldsymbol{x}_k + \boldsymbol{B}\boldsymbol{u}_k + \boldsymbol{d} + \eta_k \boldsymbol{A}_c \delta\boldsymbol{c}_i, \tag{8}
$$

where the subscript $i \in \{1, 2\}$ indicates the order of the steps. There can be either one or two scheduled steps within the prediction horizon, which is usually chosen to be slightly longer than the stance time in practice. Such choice helps to mitigate excessively aggressive stepping, because when the next scheduled step is forthcoming, another stepping opportunity will appear towards the end of the prediction horizon.

In addition, having $\delta\boldsymbol{c}$ as part of the decision variables enables the robot to negotiate sloped terrains. Suppose the nearby terrain can be estimated as a plane $\mathcal{P}$, then the following linear equality can be imposed one new step location

$$
\boldsymbol{c}_t + \delta\boldsymbol{c}_i \in \mathcal{P} := \{\boldsymbol{c} \in \mathbb{R}^3 | \boldsymbol{A}_\mathcal{P} \cdot \boldsymbol{c} = \boldsymbol{b}_\mathcal{P}\}, \tag{9}
$$

where $\boldsymbol{c}_t$ is the current step location; $\boldsymbol{A}_\mathcal{P}, \boldsymbol{b}_\mathcal{P}$ parametrizes the plane approximation of the terrain arounx $\boldsymbol{c}$. $\mathcal{P}$ can be updated iteratively to generalize the LMPC to arbitrary uneven terrains, such as the wavefield shown in Fig. 1.

Kinematic reachability constraints can also be enforced. The step size is bounded to prevent the robot from taking too large a step

$$|\delta \boldsymbol{c}_i| \leq i \cdot \delta \boldsymbol{c}_{max}, i \in \{1, 2\} \qquad (10)$$

where the step order index i scales the maximum step size $\delta \boldsymbol{c}_{max}$ proportionally. That is because $\delta \boldsymbol{c}_2$ is defined as the vector pointing from the current step location to the second predicted step location. Furthermore, leg over-extension is prevented by imposing constraints on $\boldsymbol{r}$, the vector from the CoM to the step location. At time step k, $\boldsymbol{r}_k = \boldsymbol{c} + \delta \boldsymbol{c}_i - \boldsymbol{p}_{c,k}$ is bounded by

$$|\boldsymbol{r}_k^{x/y}| \leq r_{max}^{x/y} + (1 - \eta_k) \cdot M_b, k = 1, \cdots, N_{le}, \qquad (11)$$

where $r_{max}^{x/y}$ is the maximum displacement of the new step from the CoM projection on the ground plane; η_k is the binary indicator as in (8); M_b is a sufficiently large positive number such that constraint (11) is only activated when the robot is scheduled to take a step ($\eta_k = 1$). To prevent over-constraining the optimization, (11) is only imposed for a few steps $N_{le} < N$, where the state prediction from the linearized SRB model is sufficiently accurate.

D. Line-Foot Contact

The MIT Humanoid has under-actuated feet that make line contacts with the ground. When in a single stance, the foot in contact cannot generate a moment in the *roll* direction of the foot frame $\{F\}$. As a special case in [19], the contact wrench cone (CWC) constraints of line-contact requires

$$0 \leq F_z \leq F_z^{max}, \ |F_{x,y}| \leq \mu \cdot F_z, \ m_x = 0,$$
$$- F_z \cdot l_t \leq m_y \leq F_z \cdot l_h, \qquad (12)$$

where μ is the coefficient of friction; l_h and l_t are the lengths from the origin of $\{F\}$ to the heel and toe, respectively; F_z^{max} is the maximum vertical ground reaction force; To derive the constraints on m_z, consider the GRW is instead produced by two point forces at the heel $\boldsymbol{F}^h$ and toe $\boldsymbol{F}^t$. Solving the following equations

$$F_y = F_y^h + F_y^t, m_y = F_z^h \cdot l_h - F_z^t \cdot l_t$$
$$F_z = F_z^h + F_z^t, m_z = F_y^t \cdot l_t - F_y^h \cdot l_h, \qquad (13)$$

and plugging the expressions of $F_y^h, F_y^t, F_z^h, F_z^t$ to the friction constraint $|F_{x,y}^{h/t}| \leq \mu F_z^{h/t}$, one can derive the linear inequality constraints on m_z. Collecting all linear inequalities related with line-foot contact to matrices $\boldsymbol{A}_{cwc}$ and $\boldsymbol{b}_{cwc}$, the admissible control set $\mathbb{U}$ can be defined as $\{\boldsymbol{u} \mid \boldsymbol{A}_{cwc} \cdot {}^F\boldsymbol{u} \leq \boldsymbol{b}_{cwc}\}$. The proposed LMPC works for robots with point foot or passive ankle by shrinking l_h, l_t to zero. The additional control authority of line-contact contributes to stabilizing the dynamical effects that are not captured by the SRB model.

III. HUMANOID MODEL AND CONTROL

A. Humanoid Model

The MIT Humanoid is a 24 kg robot with high torque density and high bandwidth control capability. The humanoid model has 24 degrees of freedom (DoF), with 18 actuated DoFs (5 DoFs for each leg and 4 DoFs for each arm) and the floating base coordinate. The robot configuration is described by $\boldsymbol{q} = [\boldsymbol{q}_b^\top, \boldsymbol{q}_a^\top]^\top$, where $\boldsymbol{q}_b$ is the un-actuated torso pose and $\boldsymbol{q}_a$ is the configuration of the actuated joints. The standard dynamic equations of motion are

$$\boldsymbol{H}(\boldsymbol{q})\ddot{\boldsymbol{q}} + \boldsymbol{C}(\boldsymbol{q}, \dot{\boldsymbol{q}}) = \boldsymbol{S}_a^\top \boldsymbol{\tau} + \boldsymbol{J}_c^\top(\boldsymbol{q})\boldsymbol{u}, \qquad (14)$$

where $\boldsymbol{H} \in \mathbb{R}^{n \times n}$ is the mass matrix; $\boldsymbol{C}(\boldsymbol{q}, \dot{\boldsymbol{q}})$ incorporates the centripetal, Coriolis and gravitational terms; $\boldsymbol{u} \in \mathbb{R}^6$ is the GRW and $\boldsymbol{J}_c \in \mathbb{R}^{6 \times n}$ is the corresponding contact Jacobian matrix. The matrix $\boldsymbol{S}_a = [\boldsymbol{0}^{18 \times 6}, \boldsymbol{1}^{18 \times 18}]$ is the selection matrix for the actuated joint torque vector $\boldsymbol{\tau} \in \mathbb{R}^{18}$. The humanoid model is constructed using Spatial_V2 [20] with rotor inertia.

The humanoid model is utilized in a low-level controller to track the tasks produced by the LMPC while exploiting the full-body dynamics of the humanoid robot.

B. Adaptive Gait Frequency

Adapting gait frequency is a crucial aspect of robust bipedal walking. Prior works on step timing and duration adaptation [21], [22] rely on LIPM, which is not applicable in this work. Hence, a heuristic adaptive gait frequency (AGF) scheme is presented in this section to augment the optimization-based LMPC. The design of AGF is an open-ended question since it is based on heuristic rules. Some example heuristics are: return to the nominal gait frequency by default; increase gait frequency when torso acceleration $\ddot{\boldsymbol{p}}_c$ is high due to external push; decrease gait frequency as the angular momentum increases since it is likely to be induced by fast-moving limbs. The following rule encodes the aforementioned heuristics

$$\dot{K} = C_k(1 - K) + C_{\ddot{p}_c}||\ddot{\boldsymbol{p}}_c||^2 - C_{k_G}||\boldsymbol{k}_G||^2$$
$$\dot{K}_{lb} \leq \dot{K} \leq \dot{K}_{ub}, K_{lb} \leq K \leq K_{ub}, \qquad (15)$$

where K is a gait frequency scaling factor; scalars $C > 0$ are user-tuned parameters; subscripts lb and ub represent the lower and upper bounds, respectively. Note that the factor K scales both the gait frequency and the prediction step time. Namely, $K > 1$ shortens the prediction horizon and vice versa.

IV. RESULTS

A. Simulation Setup

The full-body dynamics simulation is performed in MATLAB using $ode45$ with an event-driven finite state machine, and robot motion is visualized in Unity. Gaussian noise based on the sensor hardware is injected into the state measurement for realistic simulations.
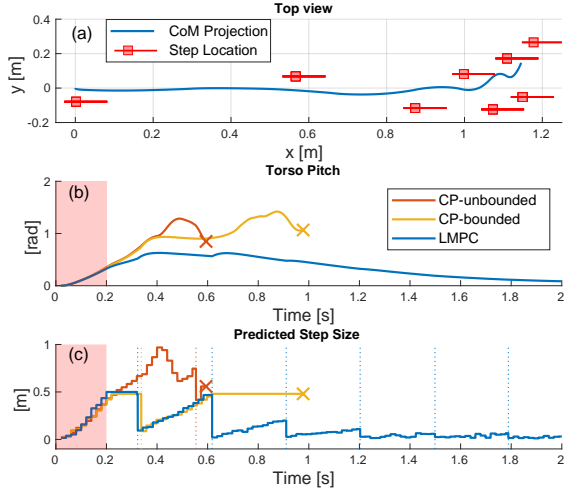
Fig. 2: Comparison of stepping strategies in a push recovery scenario. (a) The CoM position from the LMPC case is projected to the x-y plane as the blue curve; the red square indicates the foostep location, and the red line segment represents the foot in contact. (b) Torso pitch angle (c) Predicted step size. The crosses indicate that the robot fell over. The red shaded area represents a disturbance impulse of 28 Ns over 200 ms.

B. Disturbance Recovery

To show the advantage of footstep location optimization in LMPC, the following three stepping strategies are compared:

- (CP-unbounded) Capture point without kinematic limit
- (CP-bounded) Capture point with max. stride length
- (LMPC) Step location generated by LMPC

The CP stepping policy based on a 3D LIPM with point foot is used in this experiment. The CP-unbounded policy directly tracks the CP, whereas the CP-bounded policy tracks the CP up to a maximum stride length threshold to ensure kinematic feasibility. In contrast, LMPC regularizes the footstep location by penalizing e_c in the cost function.

The robot stands still on flat ground, and a disturbance is applied at the top of the torso in the forward direction. The push force is 140 N and lasts for 200 ms, an impulse of 28 Ns. The commanded velocity is zero, so the robot tries to maintain balance and come to a stop. Fig. 2 (a) displays the recovery motion of LMPC. As shown in Fig. 2 (b), CP-unbounded failed since the desired footstep location is beyond the kinematic limit of the robot. Fig. 2 (c) reveals that although CP-bounded satisfies the kinematic feasibility, the robot fell due to an over-tilted posture. In comparison, the LMPC survived the push since it can reason about the complex coupling effects among stepping, torso rotation, and contact wrench while respecting the kinematic limit.

C. Traversing Wave Field

The proposed framework enables the MIT Humanoid to walk across a wave field, as shown in Fig. 1. A sine function with increasing magnitude parametrizes the terrain profile. Although the robot is not provided with the terrain profile
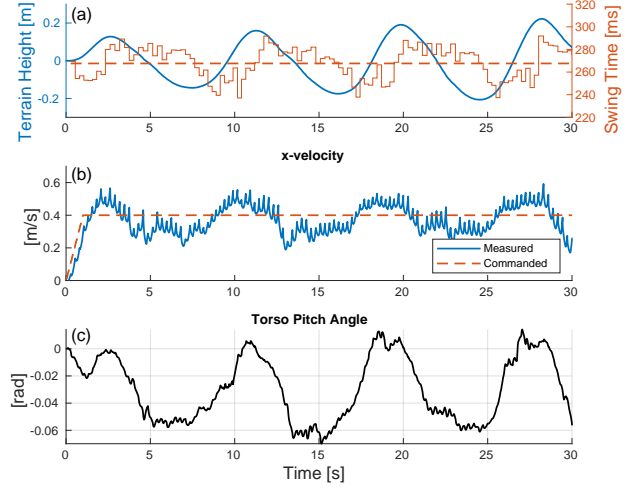

Fig. 3: Simulation result where the MIT Humanoid traverses the wave field shown in Fig. 1. (a) The swing time (red) changes with the terrain profile (blue), where the red dashed line marks the average swing time. (b) The commanded (red dashed line) and measured (blue) forward velocity; (c) Torso pitch angle.

from vision, it uses proprioceptive sensors, including the ankle encoder, to estimate the terrain slope at the contact point. Assuming the terrain height varies only in the sagittal plane, the LMPC locally linearizes the smooth terrain as a tangent plane, on which the footstep location is planned. This terrain approximation is updated as the next contact is established with the terrain surface.

V. CONCLUSION

The paper presents an LMPC-based locomotion controller that enables dynamic walking with the MIT Humanoid. Its major feature is the ability to reason the complex coupling among important aspects of humanoid walking in a unified optimization framework. Specifically, the footstep location is produced by the LMPC while considering contact wrench, torso rotational dynamics, and varying CoM height. The solution from the LMPC is posed as tracking tasks and passed down to a task-space controller to leverage the full-body dynamics of the robot. Both the LMPC and TSC are amenable for real-time applications since they can be transcribed to QP problems. In addition, a gait frequency adaptation scheme is employed to further enhance the robustness of the walking controller. The proposed framework enables the MIT Humanoid to recover from substantial disturbance and traverse a wave field.

REFERENCES

[1] Y. Ding, C. Khazoom, M. Chignoli, and S. Kim, "Dynamic walking with footstep adaptation on the mit humanoid via linear model predictive control," in *Proc. IEEE/RSJ Int. Conf. Intell. Robot. Syst. (IROS)*. IEEE, 2022, (under review).

[2] S. Kajita and K. Tani, "Study of dynamic biped locomotion on rugged terrain-derivation and application

of the linear inverted pendulum mode," in *Proc. IEEE Int. Conf. Robot. Automat. (ICRA)*. IEEE Computer Society, 1991, pp. 1405–1406.

[3] J. Yamaguchi, E. Soga, S. Inoue, and A. Takanishi, "Development of a bipedal humanoid robot-control method of whole body cooperative dynamic biped walking," in *Proc. IEEE Int. Conf. Robot. Automat. (ICRA)*, vol. 1, 1999, pp. 368–374.

[4] T. Takenaka, T. Matsumoto, and T. Yoshiike, "Real time motion generation and control for biped robot-1 st report: Walking gait pattern generation," in *Proc. IEEE/RSJ Int. Conf. Intell. Robot. Syst. (IROS)*, 2009, pp. 1084–1091.

[5] P.-B. Wieber, R. Tedrake, and S. Kuindersma, "Modeling and control of legged robots," in *Springer handbook of robotics*. Springer, 2016, pp. 1203–1234.

[6] P.-B. Wieber, "On the stability of walking systems," in *Proc. Int. Workshop Humanoid Human Friendly Robotics*, 2002, pp. 53–59.

[7] J. Pratt, J. Carff, S. Drakunov, and A. Goswami, "Capture point: A step toward humanoid push recovery," in *Proc. IEEE/RAS Int. Conf. Humanoid Robot. (Humanoids)*, 2006, pp. 200–207.

[8] T. Koolen, T. de Boer, J. Rebula, A. Goswami, and J. Pratt, "Capturability-based analysis and control of legged locomotion, Part 1: Theory and application to three simple gait models," *Int. J. Robot. Res. (IJRR)*, vol. 31, no. 9, pp. 1094–1113, Aug. 2012.

[9] B. Stephens, "Humanoid push recovery," in *Proc. IEEE/RAS Int. Conf. Humanoid Robot. (Humanoids)*, 2007, pp. 589–595.

[10] J. Englsberger, T. Koolen, S. Bertrand, J. Pratt, C. Ott, and A. Albu-Schäffer, "Trajectory generation for continuous leg forces during double support and heel-to-toe shift based on divergent component of motion," in *Proc. IEEE/RSJ Int. Conf. Intell. Robot. Syst. (IROS)*. IEEE, 2014, pp. 4022–4029.

[11] O. E. Ramos and K. Hauser, "Generalizations of the capture point to nonlinear center of mass paths and uneven terrain," in *Proc. IEEE/RAS Int. Conf. Humanoid Robot. (Humanoids)*, 2015, pp. 851–858.

[12] M. Neunert, M. Stäuble, M. Giftthaler, C. D. Bellicoso, J. Carius, C. Gehring, M. Hutter, and J. Buchli, "Whole-body nonlinear model predictive control through contacts for quadrupeds," *IEEE Robot. Automat. Lett. (RA-L)*, vol. 3, no. 3, pp. 1458–1465, 2018.

[13] G. Bledt and S. Kim, "Implementing regularized predictive control for simultaneous real-time footstep and ground reaction force optimization," in *Proc. IEEE/RSJ Int. Conf. Intell. Robot. Syst. (IROS)*, 2019, pp. 6316–6323.

[14] A. K. Valenzuela, "Mixed-Integer Convex Optimization for Planning Aggressive Motions of Legged Robots Over Rough Terrain," Ph.D. dissertation.

[15] G. P. McCormick, "Computability of global solutions to factorable nonconvex programs: Part I—convex underestimating problems," *Mathematical programming*, vol. 10, no. 1, pp. 147–175, 1976.

[16] S. Boyd and L. Vandenberghe, *Convex optimization*. Cambridge university press, 2004.

[17] P. M. Wensing and D. E. Orin, "Generation of dynamic humanoid behaviors through task-space control with conic optimization," in *Proc. IEEE Int. Conf. Robot. Automat. (ICRA)*, 2013, pp. 3103–3109.

[18] M. Chignoli, D. Kim, E. Stanger-Jones, and S. Kim, "The MIT humanoid robot: Design, motion planning, and control for acrobatic behaviors," in *Proc. IEEE/RAS Int. Conf. Humanoid Robot. (Humanoids)*, 2021.

[19] S. Caron, Q.-C. Pham, and Y. Nakamura, "Stability of surface contacts for humanoid robots: Closed-form formulae of the contact wrench cone for rectangular support areas," in *Proc. IEEE Int. Conf. Robot. Automat. (ICRA)*, 2015, pp. 5107–5112.

[20] R. Featherstone, *Rigid body dynamics algorithms*. Springer, 2014.

[21] Z. Aftab, T. Robert, and P.-B. Wieber, "Ankle, hip and stepping strategies for humanoid balance recovery with a single model predictive control scheme," in *Proc. IEEE/RAS Int. Conf. Humanoid Robot. (Humanoids)*, 2012, pp. 159–164.

[22] M. Khadiv, A. Herzog, S. A. A. Moosavian, and L. Righetti, "Walking control based on step timing adaptation," *IEEE Trans. Robot. (T-RO)*, vol. 36, no. 3, pp. 629–643, 2020.